Article ID: 1006-8775(2023) 01-0115-13

Analysis of Precipitation Anomaly and a Failed Prediction During the Dragon-boat Rain Period in 2022

DONG Shao-rou (董少柔)[1], YANG Song (杨 崧)[2, 3], LIU Wei (刘 尉)[1], HU Ya-min (胡娅敏)[1], WANG Ming-sheng (汪明圣)[1], LIU Yan (刘 燕)[4]

(1. Guangdong Climate Center, Guangzhou 510641 China; 2. School of Atmospheric Sciences and Guangdong Province Key Laboratory for Climate Change and Natural Disaster Studies, Sun Yat-sen University, Zhuhai, Guangdong 519000 China; 3. Southern Marine Science and Engineering Guangdong Laboratory (Zhuhai), Zhuhai, Guangdong 519082 China; 4. Guangdong Meteorological Society, Guangzhou 510080 China)

Abstract: This study investigates the possible causes for the precipitation of Guangdong during dragon-boat rain period (DBRP) in 2022 that is remarkably more than the climate state and reviews the successes and failures of the prediction in 2022. Features of atmospheric circulation and sea surface temperature (SST) are analyzed based on several observational datasets for nearly 60 years from meteorological stations and the NCEP/NCAR Global Reanalysis Data. Results show that fluctuation of the 200-hPa westerly wind as well as the westerly jet is strengthened due to the propagation of wave energy, leading to strong updraft over southern China. Activities of a subtropical high and a shear line provide favorable conditions for the transport of moisture to Guangdong. With the support of powerful southwest winds, extreme precipitation is induced. ENSO is a good indicator of atmospheric circulation at mid-and high-levels during the DBRP in 2022 but it performs badly at low levels. During recent years, the influence of ENSO on precipitation during the DBRP has decreased obviously. The SSTA of tropical southeast Atlantic (SEA) in spring may become the key indicator. During the years with warm SEA, wave trains propagate from northwest to southeast over Eurasia with energy enhancing the westerly jet, conducive to updraft over southern China and the occurrence of heavy precipitation. Meanwhile, the Rossby wave is triggered over Maritime Continent by heat sources of southern Atlantic-western Indian Ocean through the Gill response. Thus, strong transport of moisture and heavy rainfall occur.

Key words: dragon-boat rain period (DBRP); precipitation; ENSO; climate prediction; SSTA

CLC number: P466 **Document code:** A

Citation: DONG Shao-rou, YANG Song, LIU Wei, et al. Analysis of Precipitation Anomaly and a Failed Prediction During the Dragon-boat Rain Period in 2022 [J]. Journal of Tropical Meteorology, 2023, 29(1): 115-127, https://doi. org / 10.46267/j.1006-8775.2023.009

1 INTRODUCTION

The first annual rainy season (FARS) over southern China is from April to June, during which the precipitation is characterized of uneven spatial and temporal distribution (Wu and Liang [1]; Zhao and Chen [2]; Zheng et al. [3]). The temporal variability of the FARS mainly consists of subseasonal and interannual time scales (Xin et al. [4]; Gu and Ji [5]). It is also pointed out that the precipitation in southern China during the FARS exhibits a significant interdecadal transition from a dry state to a wet state in the early 1990s (Li et al. [6]). Precipitation in southern China during the FARS generally peaks from late May to mid-June when the dragon-boat race is held. Due to the concentrated, long-lasting and intense precipitation in Guangdong from 21 May to 20 June, this period is therefore named dragon-boat rain period (DBRP) (Qian et al. [7]; Zhang et al. [8]; Chen and Zhai [9]; Tang et al. [10]). Precipitation during this period is not only related to early rice yield and water levels, but also linked to heavy rainfall and floods. Moreover, it has an important influence on economic development and people's livelihood in Guangdong (Huang et al. [11]; Li et al. [12]). For example, characterized by long duration, high intensity and wide range of influence, precipitation during the DBRP in 2008 broke the record and caused great economic loss in agriculture, forestry, aquatic products, and transportation (Lin et al. [13]). The formation mechanism of precipitation during the DBRP is complex and the corresponding configuration of weather systems exhibits clear difference (Zheng et al. [3]; Lin et al. [13]; Wu et al. [14]). Thus, prediction of precipitation during the

Received 2022-09-30; **Revised** 2022-11-15; **Accepted** 2023-02-15

Funding: National Natural Science Foundation of China Meteorological Joint Fund(U2142205); National Key Research and Development Program of China (2018YFA0606203); Guangdong Major Project of Basic and Applied Basic Research (2020B0301030004); Guangdong Province Key Laboratory for Climate Change and Natural Disaster Studies (2020B1212060025); Innovation Group Project of Southern Marine Science and Engineering Guangdong Laboratory (Zhuhai) (311021001)

Biography: DONG Shao-rou, engineer, primarily undertaking research on climate prediction and urban climate.

Corresponding author: YANG Song, e-mail: yangsong3@mail.sysu.edu.cn

DBRP is the key difficult part of climate prediction.

By now, there have been some analysis on individual cases of the DBRP. Lin et al. [13] indicated that the extreme precipitation was associated to a weak and eastward subtropical high as well as an evident low-level jet in 2008. Gu and Zhang [15] investigated the relationship between precipitation and corresponding atmospheric low-frequency oscillation during the DBRP in 2008. Gu and Ji [5] further demonstrated the influence of atmospheric circulation at the middle and low troposphere on precipitation based on the quasi-10-day time scale. Wen et al. [16] analyzed the connection between consistent precipitation and 30–60-day oscillation in June 2005. Other research mainly focuses on statistical characteristics of annual precipitation during the DBRP and corresponding atmospheric circulation systems. By studying three types of spatial distribution of precipitation during the DBRP, Hu et al. [17] investigated the critical impact of different configurations of atmospheric circulation on the precipitation. Wu et al. [14] showed that both a weak South Asia high and a weak subtropical high were conducive to precipitation during the DBRP based on analysis in the past 55 years. Chen et al. [18] found the modulating effect of low-frequency oscillation on persistent rainstorms. Lin et al. [19] pointed out that the amount of precipitation of Guangdong in June during the past 30 years was related to the phase of MJO and its corresponding circulation characteristics. However, there are relatively few studies on the influence of sea surface temperature (SST) on the precipitation of Guangdong during the DBRP.

Compared with atmospheric circulation, the SST changes slowly and is used as an important forewarning factor in precipitation forecast. Many studies have explored the influence of the SST on the precipitation in southern China during the FARS. For example, cooler sea areas near southern China may lead to less precipitation there during the FARS (Ma et al. [20]); a warm Indian Ocean may weaken the impact of summer monsoon on the precipitation over southern China (Yang et al. [21]; Li et al. [22]); Probability of extremely dry or wet conditions in southern China from May to June may increase when PDO and ENSO are in the same phase (Chan and Zhou [23]); Warm SST of the South China Sea-western Pacific Ocean may facilitate persistently extreme precipitation over southern China in late spring and early summer (Hong and Ren [24]). Sea surface temperature anomaly (SSTA) in the equatorial central and eastern Pacific is the key factor in climate prediction. ENSO is an important component of climate variation and it is closely related to the East Asian summer monsoon which may have a decisive influence on the precipitation during the flood season in southern China (Chan and Zhou [23]; Zhou et al. [25]; Chang et al. [26]; Yim et al. [27]).

Cold events successively occurred twice from 2020 to 2022, which is historically rare. Moreover, the precipitation of Guangdong during the DBRP in 2022 was so heavy that it ranked the third since 1961. However, results of precipitation prediction by many models differ greatly from the observation. Based on models and diagnosis, forecasters correctly judged the general trend of precipitation during the DBRP in 2022 but failed to predict the spatial distribution of precipitation anomaly. In this study, we analyze the possible causes for the precipitation of Guangdong during the DBRP in 2022 that is remarkably more than the climate state and review the successes and failures of the prediction, which may provide possible ways to improve climate prediction by showing typical cases for reference. The rest of this paper is organized as follows. Section 2 introduces observational data and statistical methods applied in this study. In section 3, we show the major features of the precipitation of Guangdong during the DBRP and we also compare the results between prediction and observation in 2022. Analysis on the influence by atmospheric circulation on extreme precipitation is shown in section 4. Section 5 contains the evolution of relationship between ENSO and precipitation during the DBRP and reveals a possible mechanism of how the key marine area affects the precipitation in Guangdong. A summary and a further discussion are provided in section 6.

2 DATA AND METHODS

The dataset used for the study consists of geopotential height (Z), sea level pressure (SLP), zonal and meridional winds (U, V), vertical p-velocity (omega), specific humidity (Q) fields at 2.5°×2.5° global grids from the National Centers for Environmental Prediction-National Center for Atmospheric Research (NCEP-NCAR) Reanalysis (Kalnay et al. [28]), daily rainfall data from 86 stations in Guangdong, Hadley Centre Sea Ice and Sea Surface Temperature dataset at 1° horizontal resolution (HadISST; Rayner et al. [29]). All the datasets cover the period from 1961 to 2022. The dragon-boat rain period (DBRP) is defined as a time lasting from May 21 to June 20, during which precipitation in Guangdong is highly concentrated.

The methods applied in this study include linear regression, standardization, correlation analysis, moving average, Student-t test, composite analysis, 25-year sliding correlation and Euclidean distance. During the analysis of wave-activity flux, Equation 38 by Takaya and Nakamura [30] is used and the corresponding basic flow is the climate mean between May 21 and June 20 from 1961 to 2022. The total column water vapor (W) and water vapor flux (F_x, F_y) are calculated as follows:

$$\mathrm{W} = \frac{1}{g}\int_{P_t}^{P_s} q\,\mathrm{d}p \tag{1}$$

$$F_x = \frac{1}{g}\int_{P_t}^{P_s} qu\,\mathrm{d}p \tag{2}$$

$$F_y = \frac{1}{g}\int_{Pt}^{Ps} qv\mathrm{d}p \quad (3)$$

Ps means the surface air pressure (at 1000 hPa), Pt uses the air pressure at 300 hPa due to mid-and lower-level residence of water vapor, g is the acceleration of gravity, u, v and q are the zonal and meridional winds, and specific humidity, respectively.

3 MAJOR FEATURES AND PREDICTION

According to Fig. 1a, precipitation during the DBRP in 2022 ranked the third largest since 1961. The average precipitation in Guangdong in this period is 514.5 mm, which is 54% more than the climate mean. Neither decadal features nor significant uptrends of accumulated rainfall are shown. Precipitation during the DBRP in 2022 mainly concentrated in the first half of June, during which the daily rainfall greatly exceeds the corresponding value of climatic state (Fig. 1b). It is known from the spatial distribution (Fig. 2b) that although the western part of Guangdong coast is drier, most regions of the province is extremely wet, especially the northern and eastern parts. Compared with the observation (Fig. 2b), only the wet feature and the anomaly of precipitation over the southern part of Guangdong are correctly forecast. It is unfortunate to see that the prediction of precipitation anomaly over the northern part of Guangdong differs greatly from the reality during the DBRP in 2022 (Fig. 2a).

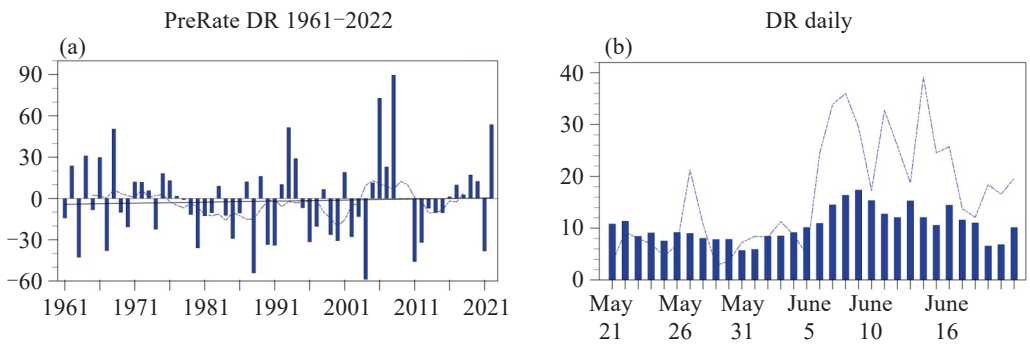

Figure 1. (a) The percentage of rainfall anomaly (blue histogram; units: %) in Guangdong during the DBRP from 1961 to 2022 (Digit on the upper right corner represents the t value, which guarantees the 95% significance of the trend only if it is greater than 1.67. The black solid line and blue dashed line represent the trends and the nine-point moving average line, respectively); (b) Daily rainfall of Guangdong province during the DBRP in 2022 (blue dashed line; units: mm) and climate state (blue histogram; units: mm).

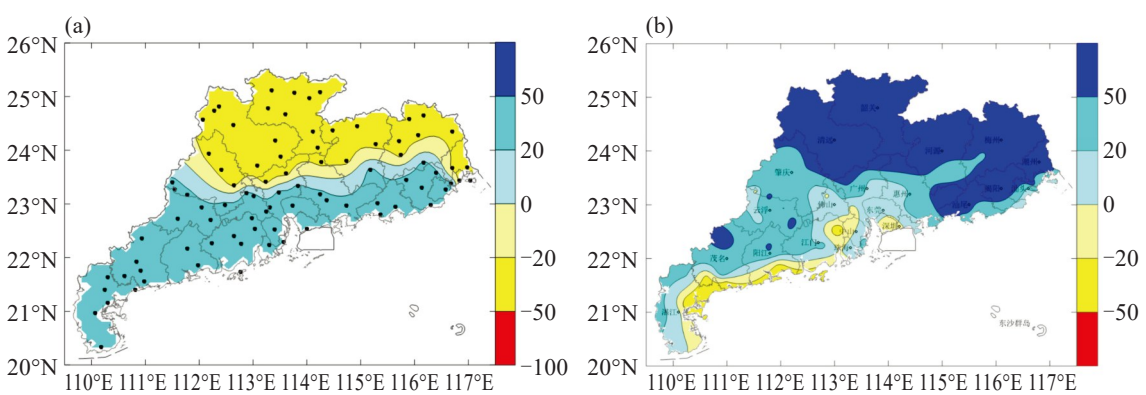

Figure 2. (a) Prediction and (b) observation of the percentage of rainfall anomaly in Guangdong during the DBRP in 2022 (units: %; scattered points represent the 86 meteorological stations in the province).

4 ATMOSPHERIC CIRCULATION

Climate prediction is made by forecasters based on objective results of numerical models, physical and statistical correction, and the merging of various results (Zhang et al. [31]). Forecasts initialized in March by models both abroad and at home show that precipitation during the DBRP is less than the climate state over Guangdong, especially over the northern part. Moreover, forecasts initialized in April further exaggerate the dry trend during the DBRP, which is opposite to the reality. Section 4 contains an analysis of the influence of atmospheric circulation on the precipitation during the DBRP in 2022.

4.1 *Westerly jet, upper-level ridges and troughs*

Fluctuations of ridges and troughs at the upper level during the DBRP in 2022 were stronger than those in the climate state. The speed of the westerly jet was higher and a high-speed zone exceeding 40 m/s extended from 120° E to 140° W (Fig. 3a). The westerly fluctuated strongly and exhibited longwave distribution with two troughs and two ridges. According to the principle of statics, the subsidence and cold advection prevail north to the southern China region behind an upper-level

trough (Fig. 4). According to Fig. 3c, easterly anomaly covers the Arabian Sea, the Bay of Bengal, and the area to the north and it splits at 110°E into two negative belts. Thus, the westerly is weakened to the north while the easterly is strengthened to the south of the strong westerly jet from the east of China to the middle latitudes of the Pacific. Affected by geostrophic deviation winds, the updraft over southern China is accelerated (Fig. 4) to the rear-right region of the jet entrance and therefore facilitates the persistent precipitation.

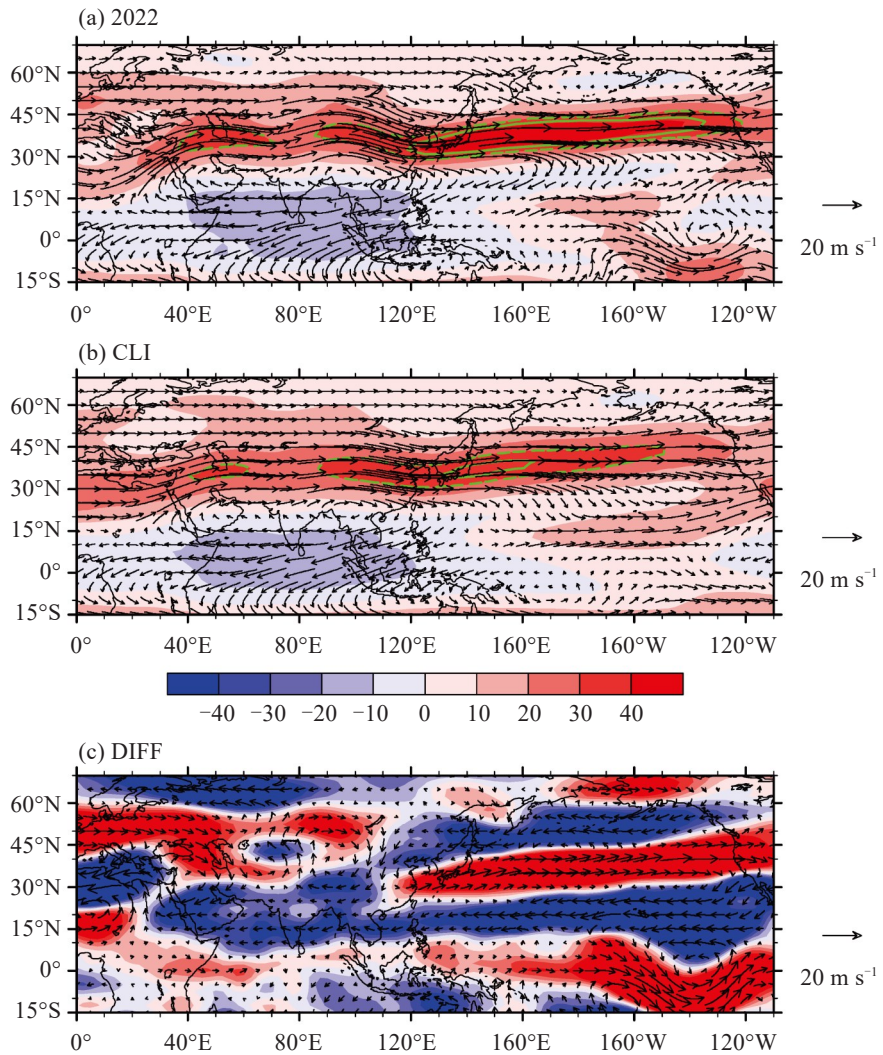

Figure 3. The 200-hPa wind vectors (units: m s^{-1}) and zonal wind (shaded; units: m s^{-1}) during the DBRP in (a) 2022 and (b) their climate state (The green dashed and solid contours represent zonal wind speeds of 30 and 40 m s^{-1}, respectively), and (c) their anomalies.

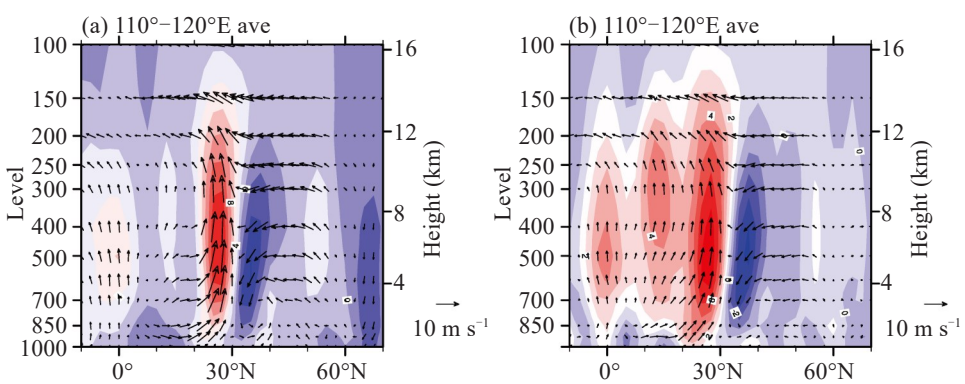

Figure 4. Vertical profile distribution of vertical *p*-velocity (−100×ω) and meridional wind averaged over 110°−120°E during the DBRP in (a) 2022 and (b) their climate state. The black vectors represent the vertical and meridional vector wind fields while the shaded parts represent the vertical *p*-velocity (units: m s^{-1}).

According to Fig. 5, atmospheric disturbance was stronger than the simultaneous climate mean during the DBRP in 2022. Compared with the climate mean state, the wave energy propagated from west to east along the middle and high latitudes over Eurasia. The northern branch of the wave activity flux propagated along the western coast of Western Europe, the West Siberian plain north of the Caspian Sea and Mongolia, and the southern branch propagated along the Mediterranean-Black Sea, east of the Caspian Sea and Xinjiang. Compared with the period when precipitation peaks from June 6 to 16 (Fig. 1b), the propagation of wave energy during late May mainly concentrated in the northern branch (figure omitted). Unstable development of the westerly belt longwave made it easy to form a cut-off low pressure, which is known as the cold vortex over the northeast of China in the middle and upper atmosphere. In short, waves were active near the jet stream and provided energy for the activities of ridges and troughs and thereby modulated the longwave.

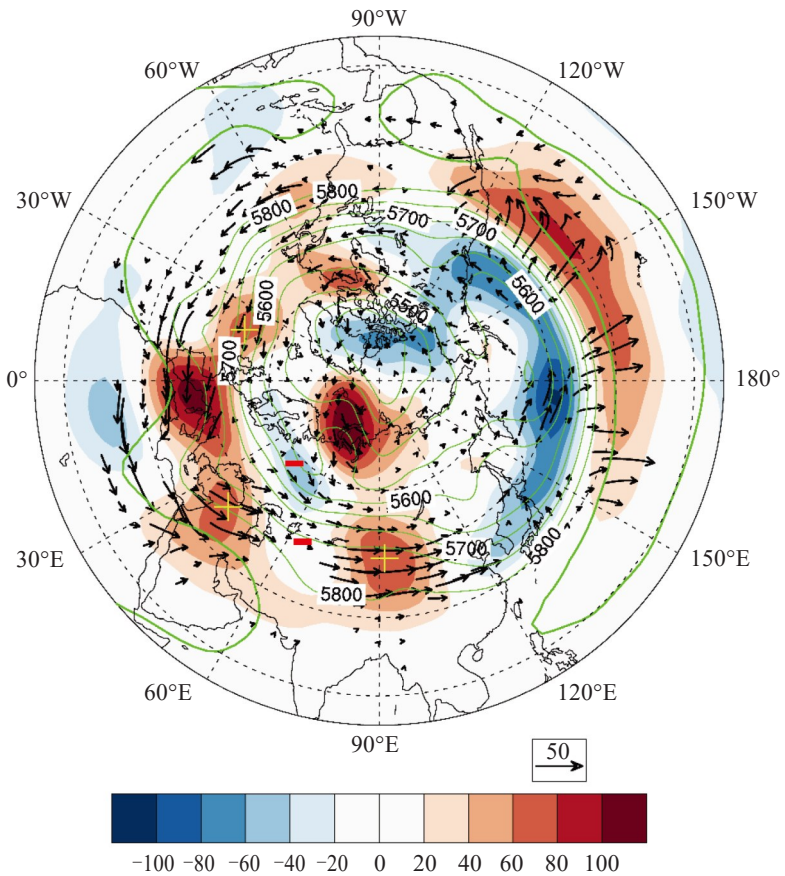

Figure 5. Geopotential height anomalies at the 200-hPa level (shaded; units: gpm) and the associated wave activity flux (vectors; units: $m^2 s^{-2}$) during the DBRP in 2022. The green contour and the bold line represent the Z500 and the 5880-gpm line, respectively. The "+" and "−" represent the positive and negative anomaly of geopotential heights, respectively.

4.2 *Activities of subtropical high*

Compared with the simultaneous climate mean, anomalies of the geopotential height exhibited a wave-train structure with the centers of "−, +, −" oriented from northwest to southeast in the upper and middle atmosphere during the DBRP in 2022 (figure omitted). Being more southward than the simultaneous climate mean state, the subtropical high retreated eastward with its westernmost ridge point changing from 108°E during early May to 122°E during late May and finally around 120° E (figure omitted). Fig. 6a shows that the subtropical high extended westward intermittently, and overall weakening and eastward retreats are found during May 21-June 5. The subtropical high extended much westward around June 5−10 and reached the westernmost position on June 10. During June 10−20 in 2022, the westernmost ridge point of the subtropical high maintained at 120° E, which was conducive to continual guiding transport of water vapor from south to north and bringing extreme precipitation (Fig. 1b). Fig. 6b reveals that the position of the subtropical high first moved north and then headed south. When the subtropical high was around 22°N with its westernmost ridge point at 120°E, the precipitation peaked during the DBRP in 2022. This special position of the subtropical high is similar to the findings of Gu and Ji [5] and Hong and Ren [24]. Moreover, each westward extension (Fig. 6a) or each northward progression (Fig. 6b) of the subtropical high perfectly coincided with the start of a new process of precipitation during the DBRP in 2022.

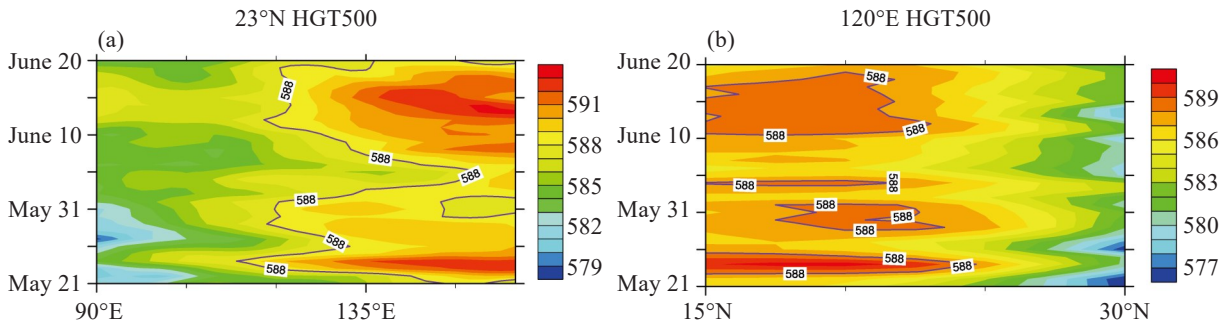

Figure 6. (a) Longitude-time cross sections at 23°N and (b) latitude-time cross sections at 120°E of Z500 during the DBRP in 2022 (shaded; units: 10 gpm). Contours are the 5880-gpm lines.

4.3 *Transport of water vapor*

The southwest winds at the 850-hPa level over Guangdong were much stronger than the climate state due to a robust flow at the edge of the Philippine anticyclone and the powerful southwesterly flow of the South China Sea. With the persistence of a shear line anomaly north of Guangdong, the transport of warm and moist currents was blocked so that the water vapor can gather over Guangdong (figure omitted). Fig. 7 further illustrates the transport of water vapor. Sources of abundant water vapor during the DBRP in 2022 include the Bay of Bengal, the South China Sea, and the western Pacific (Lin et al. [32]). The whole column of moisture transport converged over the northern part of southern China, which was much stronger than the climate state (Fig. 7a–7b). High-value centers of southerly and westerly moisture transport were dominant over Guangdong (Fig. 7c–7d), which was guaranteed by the powerful southwest winds. Transport of moisture changed from southwest to west over the northern part of Guangdong, which suggests the block of moisture by the shear line, contributes to abundant moisture over southern China, especially the northern part of Guangdong. With the guidance of the upper-level air flow and the uplifting movement at the edge of the subtropical high, ascending motion is dominant throughout the vertical layer. Thus, the precipitation during the DBRP in 2022 was persistent and extreme.

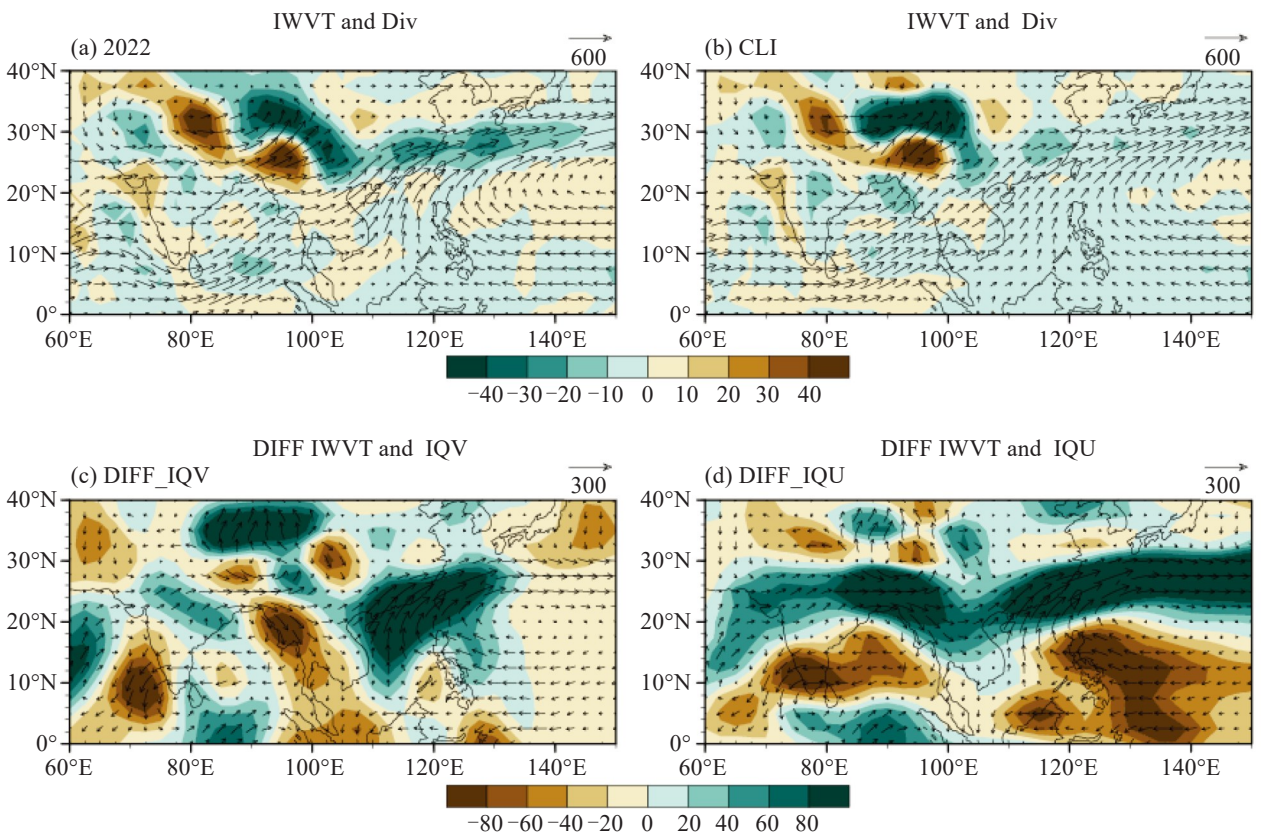

Figure 7. Total column water vapor flux (vector; units: kg m^{-1} s^{-1}) and the divergence field (shaded; units: 10^{-5} kg m^{-2} s^{-1}) during the DBRP in (a) 2022 and (b) their climate state. The anomalies of (c, d) water vapor flux (vector; units: kg m^{-1} s^{-1}), (c) meridional water vapor flux (shaded; units: kg m^{-1} s^{-1}) and (d) zonal water vapor flux (shaded; units: kg m^{-1} s^{-1}).

5 INFLUENCE OF SST

The SSTA of key areas is the important driver of atmospheric circulation anomalies (Huang and Sun [33]; Wang et al. [34]). Under the condition of successive cold events in 2022, composites of precipitation in similar years with minimum Euclidean distance of ONI (3-month moving average SSTA of 5°N−5°S, 120°−170°W) were calculated, showing spatial distribution of precipitation anomaly like that in Fig. 2a. Not only the analysis of the preceding snow and southern China summer monsoon but also the relationship between SSTA in Pacific and precipitation during the FARS (Qiang and Yang [35]) suggested dry anomaly in Guangdong. In short, they failed to provide proper guidance for precipitation prediction during the DBRP in 2022.

5.1 *Indication of ENSO evolution*

Figure 8 shows the composites of vertical profile distribution in the years with similar ONI. The whole layer over north Guangdong is dominated by downdraft while significant updraft and negative geopotential height anomaly prevails in the south. Compared with Fig. 4, the boundary between updraft and downdraft shifts southward from 30° N to 23° N, resulting in less precipitation in northern Guangdong. Composites of horizontal distribution at different levels (figure omitted) showed similar features of atmospheric circulation at the upper and middle levels during the DBRP in 2022: The upper westerly over the east of China and mid-latitude Pacific was strengthened; negative geopotential height anomaly was dominant over southern China at the 500-hPa level. At the 850-hPa level, cyclonic circulation anomaly prevailed over the South China Sea-Philippines region, which is opposite to the observation. Changes of atmospheric circulation at upper- and mid-levels are of great importance to modulating precipitation (Miao et al. [36]). The evolution of ENSO is a good indicator of atmospheric circulation at the upper- and mid-levels but it was a less useful guide for prediction of low-level atmospheric circulation during the DBRP in 2022.

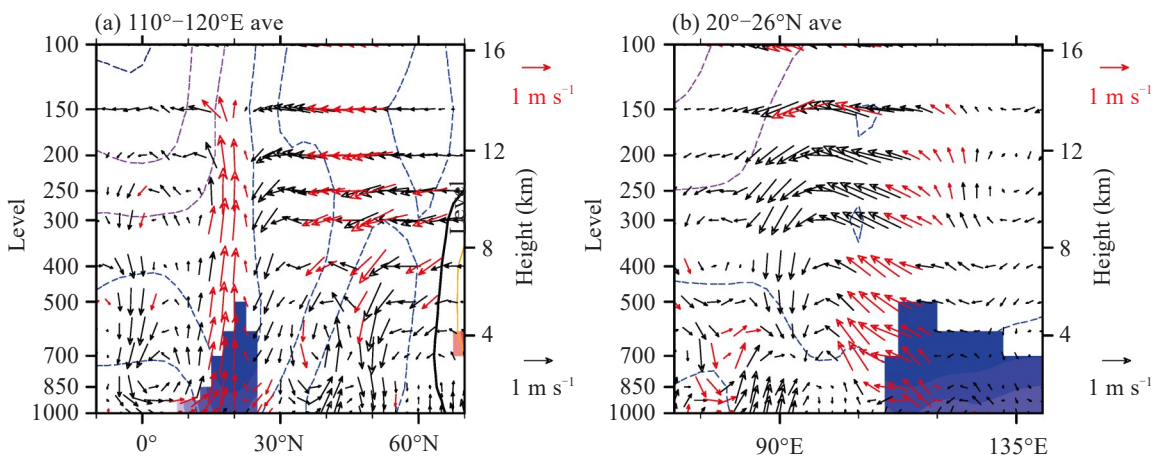

Figure 8. Vertical profile distribution of simultaneous composite of wind anomalies (black vector; units: m s^{-1}) and geopotential height anomaly (contour; units: gpm) for (a) vertical *p*-velocity (−100×ω) and meridional wind averaged over 110°−120° E, (b) vertical *p*-velocity (−100×ω) and zonal wind averaged over 20°−26°N during the most similar eight years according to ONI (2012, 1985, 2009, 2001, 1997, 1972, 1986 and 1975). The red vectors and the shades represent the 95% confidence level.

The correlation coefficient was just 0.03 between Ñino3.4 in preceding winters and the precipitation of Guangdong during the DBRP from 1961 to 2022. In order to clarify the relationship between ENSO and precipitation during the DBRP, Fig. 9 shows their sliding correlation with a 25-year window. The correlation between Ñino indexes in spring and precipitation is stronger than that in winter (Fig. 9). Moreover, positive correlations with the confidence level exceeding 95% are shown between Ñino3.4 in spring and precipitation during the DBRP from 1976 to 2006. After 2006, this positive correlation rapidly decays and strengthens reversely. In 2022, the relationship between ENSO and precipitation should be negatively correlated (Fig. 9c), namely, the negative Ñino3.4 is with the positive anomaly of precipitation. However, the negative correlation is not yet significant in 2022 and there must be another key index of SSTA.

5.2 *The tropical southeast Atlantic*

Since maximum absolute values occur in 1989 (positive correlation) and 2010 (negative correlation) by sliding correlation (Fig. 9c), the period during 1961−2022 can be divided into two parts of 1977−2001 (Period 1) and 1998−2022 (Period 2). Meanwhile, both the Ñino indexes and Indian Ocean dipole index (averaged SSTA of 30°−40°S, 60°−80°E minus averaged SSTA of 5°−35° S, 95°−115° E; figure omitted) show better relationship in springs than in preceding winters with the precipitation during the DBRP. Fig. 10a and Fig. 10c show the regression of SST in spring against the

percentage of rainfall anomaly in Guangdong during the DBRP. During Period 1, significant positive correlation is exhibited between the precipitation and SSTA of equatorial central and eastern Pacific. In Period 2, the ENSO signal decays and the significant area is replaced by tropical southeast Atlantic. The averaged SSTA of this key area (5°N−15°S, 25°W−10°E) is hence defined as the SEA index. When the SEA index is positive, significant warm SSTA occurs in tropical eastern Indian Ocean and western Pacific during Period 1 while significant warm SSTA moves westward to western Indian Ocean and Maritime Continent during Period 2 (Fig. 10b and 10d), which also reveals the weaker effect of the ENSO in Period 2. Sliding correlation between precipitation and SEA index (figure omitted) further illustrates that negative correlation peaks in 1981 and then decays before changing into positive correlation which strengthens rapidly and finally maintains at significant levels after 2008. Thus, the SEA can replace ENSO as the significant signal of precipitation during the DBRP in Period 2.

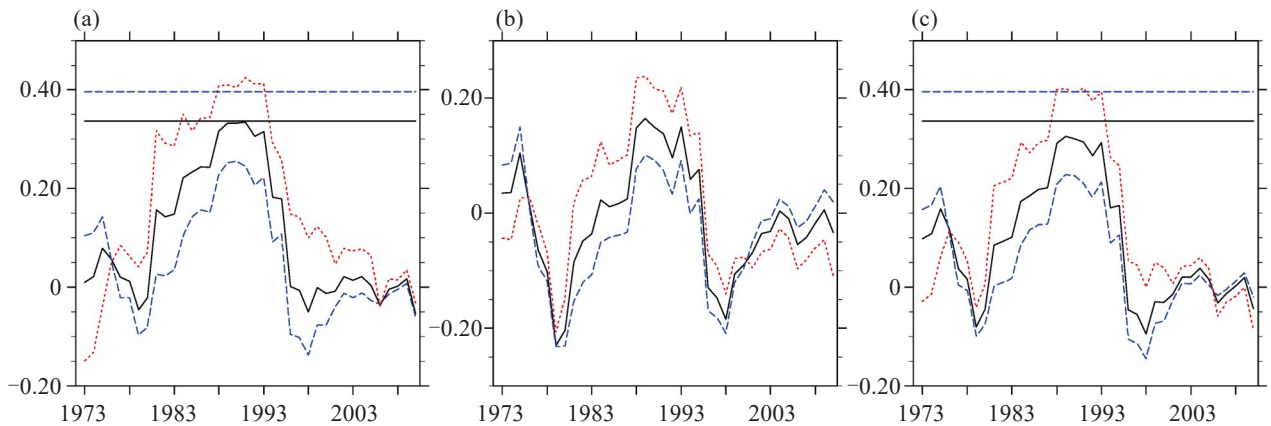

Figure 9. Sliding correlation between (a) Ñino3 (5°N−5°S, 90°−150°W averaged SSTA), (b) Ñino4 (5°N−5°S, 160°E−150°W averaged SSTA), (c) Ñino3.4 (5°N−5°S, 120°−170°W averaged SSTA) and percentage of rainfall anomaly in Guangdong during the DBRP with the center year of the 25-year window shown from 1961 to 2022. The blue lines represent the preceding winter, the black lines represent the DJFMAM (preceding winter and spring), and the red lines represent spring. The black and blue direct lines represent the 90% and 95% confidence level, respectivley.

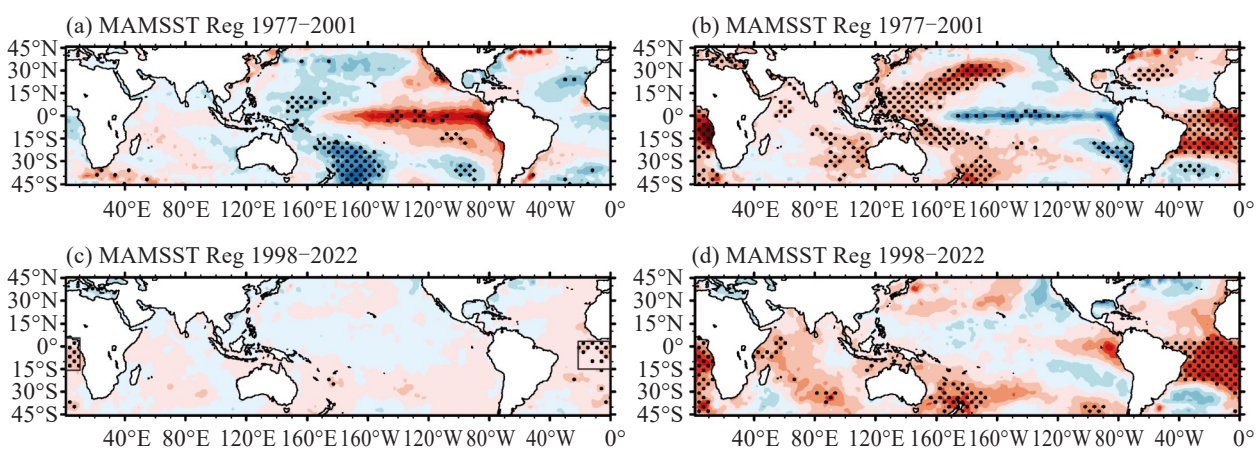

Figure 10. Regressions of SST in spring against the percentage of rainfall anomaly in Guangdong during the DBRP (a) from 1977 to 2001 and (c) from 1998 to 2022. Regressions of SST in spring against simultaneous SEA (5°N−15°S, 25°W−10°E averaged SSTA, shown in the box of (c) during (b) 1977 to 2001 and (d) 1998 to 2022. Scattered dots represent the areas where the 95% confidence level is exceeded.

Figure 11 displays correlation fields between precipitation and simultaneous atmospheric circulation at different levels during Period 1 and Period 2. According to previous studies (Wang et al. [37]; Xie et al. [38]), the Philippine anticyclone stabilizes during late autumn and early winter in El Ñino years and peaks in spring. The anticyclone is more significant in Period 1 (Fig. 11e) than in Period 2 (Fig. 11f). To the west of the equatorial heat source (Fig. 10a), the anomaly of the westerly prevails at the 850-hPa level (Fig. 11e). Significant easterly anomaly is dominant at the 200-hPa level over equatorial central Pacific (Fig. 11a) with a pair of anticyclones to the north and south. The above features of ENSO are much weakened in Period 2 (Fig.

10c, Fig. 11f and 11b), which further suggests that the impact of ENSO on the precipitation of Guangdong during the DBRP has decreased in Period 2. With low-level divergence and high-level convergence, the key area with cold SEA is dominated by downdraft in Period 1 and opposite features can be found in Period 2, which shows the response of the atmosphere to the ocean (figure omitted). Moreover, cyclones and anticyclones alternately appear over North Africa, northern Mediterranean, West Siberia, the Balkhash Lake, and eastern China (Fig. 11b and 11d) in Period 2. The wave train runs roughly from northwest to southeast (NW-SE) in the mid - and high-latitudes over Eurasia, which is consistent with the result of analysis on the wet FARS in 2010 (Miao et al. [36]). Thus, it suggests that upper-level systems may influence the precipitation during the DBRP in Period 2. In addition, the westerly prevails at high levels over equatorial eastern Indian Ocean and Maritime Continent while the easterly prevails at low levels at the southern edge of the Philippine anticyclone in Period 2. These features are all significantly stronger than those in Period 1.

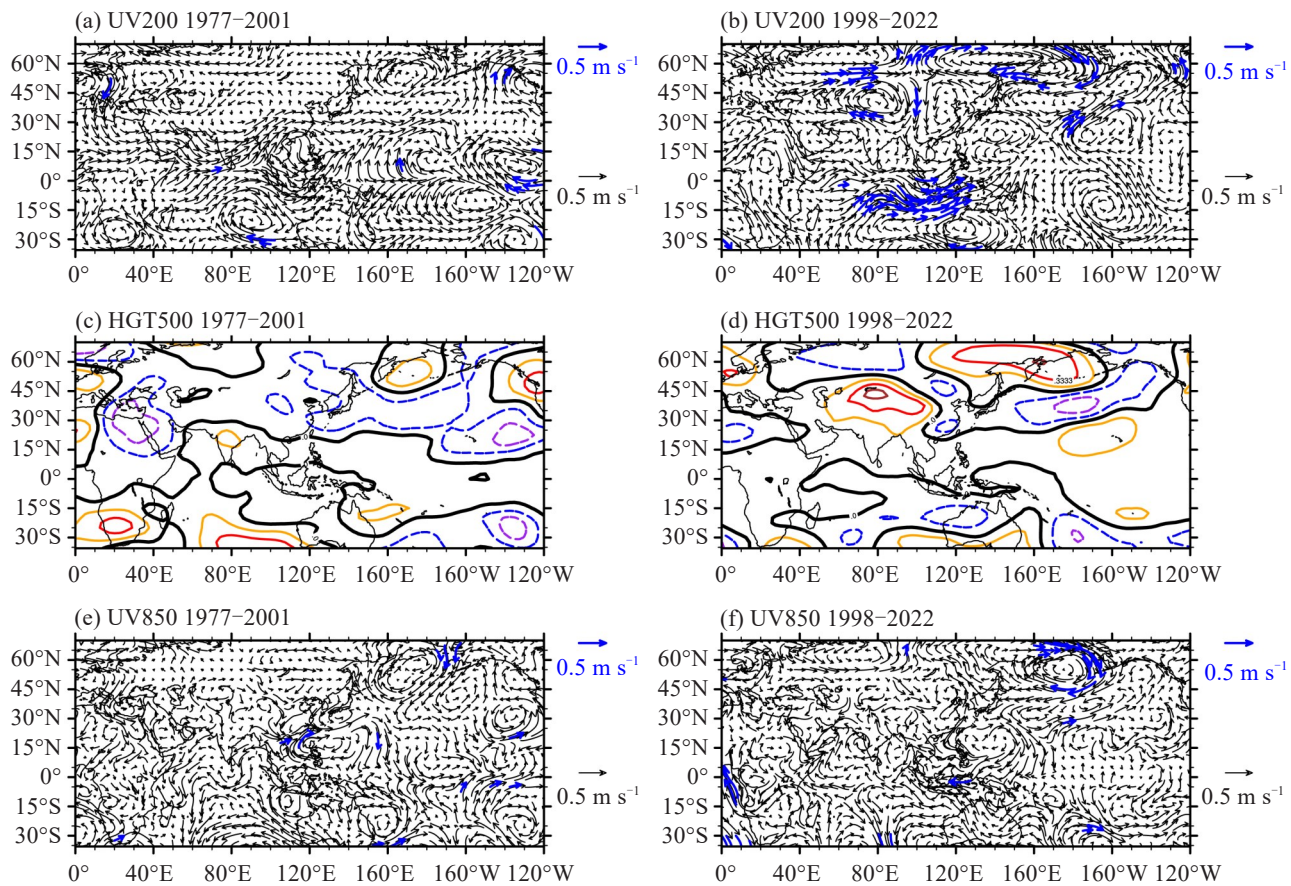

Figure 11. Correlation coefficient between the percentage of rainfall anomaly in Guangdong during the DBRP and (a, b) upper-level winds, (c, d) *Z*500, and (e, f) low level winds from 1977 to 2001 (left panels) and from 1998 to 2022 (right panels). The blue vectors represent the areas where the 95% confidence level is exceeded.

To further determine the relationship between SEA and atmospheric circulation, features at different levels in the warm-SEA years are shown in Fig. 12a−12c. According to Fig. 12a, the NW-SE wave train runs across Eurasia, which is similar to the Eurasian pattern (EU) by Wallace and Gutzler [39] and Fig. 11b. Liu et al. [40] have also pointed out the possible influence of the EU wave train on low-frequency precipitation in southern China. However, the wave train is not shown in Period 1 (figure omitted). It suggests that the warm SEA may influence the precipitation during the DBRP through an upper-level wave train. Waves are active near the jet stream and supply the energy. The climatic jet stream nuclei over Japan are superimposed at the upper level over East China, resulting in a much stronger westerly jet. Updraft is predominant to the right of the jet stream entrance over southern China (figure omitted) and precipitation is therefore enhanced. Wave activity flux during warm-SEA years (>0.5 standard deviation; figure similar to Fig. 5, omitted) further illustrates that the energy of wave propagates through Western Europe, the West Siberian plain north of the Caspian Sea and Mongolia and influences upper-level atmospheric circulation at the mid - and high-latitudes. In addition, significant westerly anomaly prevails at the 200-hPa level over equatorial eastern Indian Ocean and Maritime Continent (Fig. 12a) while significant easterly anomaly is active at the southern edge of the Philippine

anticyclone at the 850-hPa level (Fig. 12c). These features are more obvious than those in Fig. 11b and 11f. According to the composite anomalies of 200-hPa winds, 500-hPa geopotential heights and 850-hPa winds with positive years minus negative years (Fig. 12d−12f), westerly jet strengthens in the upper atmosphere and the positive center of the mid-level geopotential height anomaly is located more southward than the subtropical high of the climate state. Moreover, southern China is under the control of a low-level anticyclone and there is a significantly dominant updraft anomaly over Guangdong in the vertical profile (figure omitted). These features are consistent with those in 2022. Similar to Fig. 12a−12c and Fig. 11b, 11d and 11f, a wave train as well as the 200-hPa anomalies of westerly winds and the 850-hPa anomalies of easterly winds over Maritime Continent can all be found in Fig. 12d−12f. Meanwhile, composite anomalies at different levels of atmospheric circulation with warm-SEA years minus cold years in Period 2 are also similar to those in Fig. 12d−12f (figure omitted).

In short, warm SEA is beneficial to more precipitation during the DBRP through certain configuration of atmospheric circulation at different

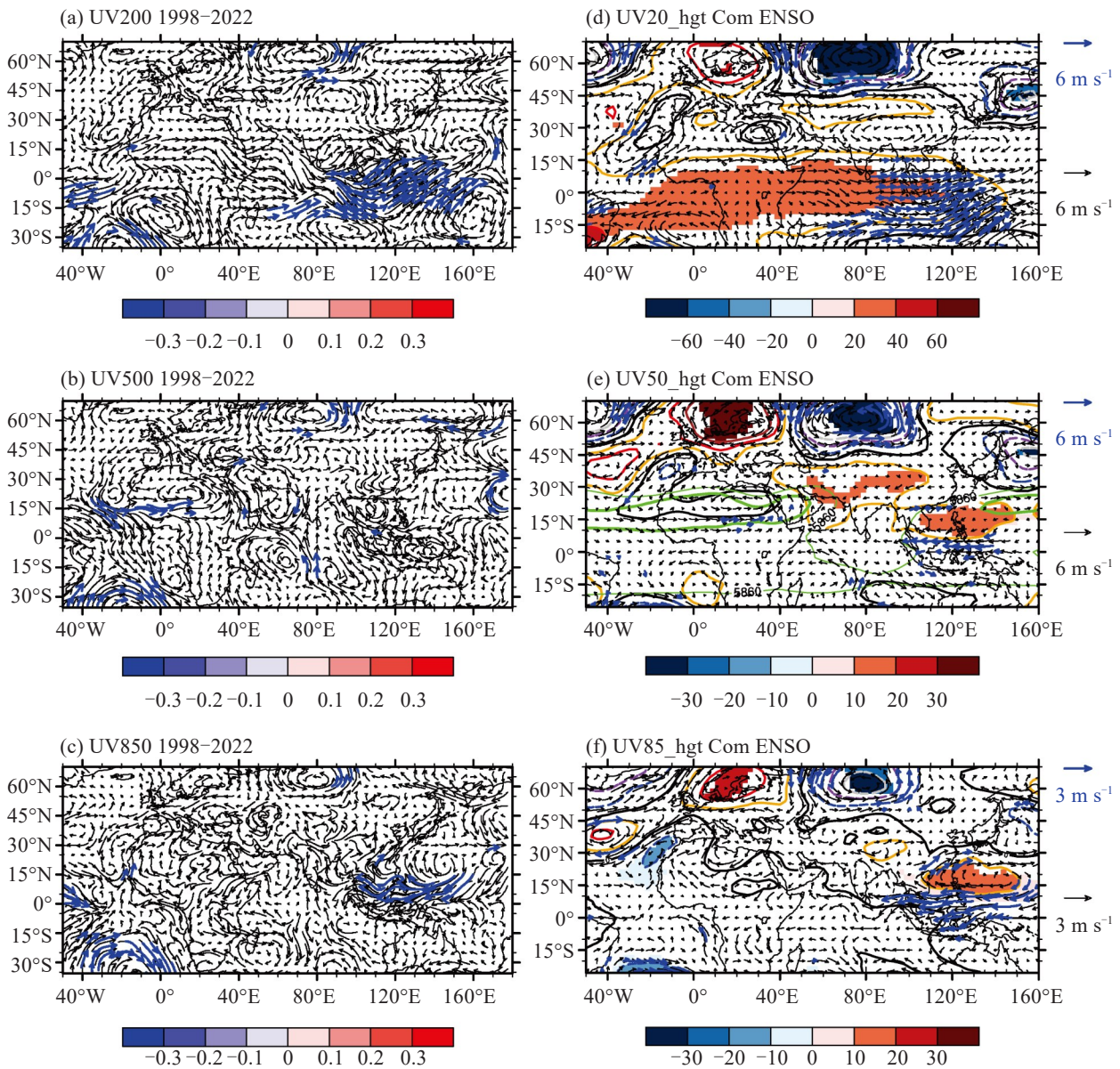

Figure 12. The left column represents the correlation coefficient between the SEA in spring and (a) 200-hPa, (b) 500-hPa, (c) 850-hPa winds from 1998 to 2022. The blue vectors represent the areas where the 95% confidence level is exceeded. The right one represents the deviation between positive years (warm SEA in spring and more precipitation during the DBRP: 1998, 2001, 2005, 2006, 2007, 2008, 2009, 2010, 2016, 2017, 2018, 2019, 2020, and 2022) and negative years (cold SEA in spring and less precipitation during the DBRP: 2004 and 2012) of composite anomalies of (d) 200-hPa, (e) 500-hPa, (f) 850-hPa winds (black vectors; units: m s^{-1}) and geopotential height (contours; units: gpm). The blue vectors and the shaded areas represent the areas where the 95% confidence level is exceeded and the green contours represent the 5880-gpm and 5860-gpm lines.

levels. During the years with warm SEA, the propagation of wave trains over Eurasia is obvious and the anomaly of cyclonic circulation controls Guangdong at the 200-hPa level. Waves are active near the jet stream and help to strengthen the westerly jet and the vertical updraft over southern China, providing necessary situation for more precipitation. Moreover, the western Indian Ocean is significantly warmer and the eastern Indian Ocean-equatorial central Pacific is colder during the warm-SEA years (Fig. 10d). Through the Gill [41] response, anomalies of westerly and easterly winds are induced to the west and east of the heat source over tropical southern Atlantic-western Indian Ocean, respectively (Fig. 12c). Anticyclone pairs can also be found to the north and south of Maritime Continent. Therefore, the response of the Rossby wave can enhance the southwest transport of moisture. Besides, direct thermal circulation causes subsidence over the cooler eastern Indian Ocean-western Pacific and updraft over southern China. Finally, precipitation during the DBRP is abundant.

6 CONCLUSIONS AND DISCUSSION

This study analyzes the main factors of atmospheric circulation and SST for abnormal precipitation of Guangdong during the DBRP in 2022. We also summarize the successes and failures of the prediction in 2022. The conclusions are as follows:

(1) Fluctuation of the 200-hPa ridge and trough is obvious during the DBRP in 2022 with the propagation of wave energy, which enhances the westerly jet and further leads to stronger updraft over southern China. During the peak stage of the DBRP, the subtropical high persists near 120° E and provides favorable conditions for the occurrence of precipitation, which include upward movement and transport of moisture at the edge of the high. Moisture is transported to southern China by strong southwest winds and is intercepted and collected by a shear line to the north of Guangdong. All these features contribute to extreme precipitation during the DBRP in 2022.

(2) ENSO is valuable for the prediction of atmospheric circulation at mid - and high-levels during the DBRP but its indication of contemporaneous precipitation in current years is decreasing obviously. The SSTA of tropical southeast Atlantic gradually becomes the key indicator.

(3) During the years with warm SEA, a NW-SE wave train appears over Eurasia at mid - and high-levels with the propagation of the wave energy enhancing the westerly jet, being conducive to the updraft over southern China and the occurrence of heavy precipitation. Meanwhile, tropical heat sources move westward to southern Atlantic-western Indian Ocean to trigger the Rossby wave over Maritime Continent through the Gill response, resulting in strong moisture transport to Guangdong and therefore inducing heavy rainfall.

To further verify these results, this study also analyzes corresponding atmospheric circulation and SSTA in 2006 and 2008 when precipitation ranked the second and the first during the DBRP, respectively. Many similar characteristics can be found. In 2006, ascending motion was more significant than that in 2022. Fluctuations of westerly winds in 2006 were strong and exhibited longwave distribution with two troughs and two ridges with a strengthened westerly jet, which are almost the same to those in 2022. Moreover, the northern branch of the wave activity flux propagated and converged more strongly. In 2008, the ascending motion was even stronger and the fluctuation of westerly winds was of longwave with only one trough and one ridge with an extremely strong westerly jet core. The anomaly of zonal wind in 2008 showed similar distribution as that in Fig. 3c. Similarly, moisture was transported to southern China by strong southwest winds and was intercepted and collected by shear lines in these three years. In addition, wave-train structures from northwest to southeast in the upper and middle atmosphere during the DBRP in 2006 and 2008 were also evident, which were consistent with warm SSTAs in tropical southeast Atlantic in both years. In 2006, preceding negative SSTA in equatorial central and eastern Pacific and more precipitation during the DBRP also show that the positive correlation between ENSO and precipitation in Guangdong has decayed. In 2008, precipitation during the DBRP was quite heavy after the peak of the cold event, which further suggests the development of negative correlation.

There are many uncertain factors in climate prediction, from which forecasters need to distinguish available signals according to their features during different stages. In addition, detailed diagnosis and analysis of atmospheric circulation are necessary. Systematic diagnosis can help forecasters better capture the overall trend of precipitation even if most results of models are completely contrary to the reality. Prediction of extreme precipitation during the FARS is the difficult part in climate prediction. This study supplements the past research with a new typical case in 2022 and issues some new arguments. For example, it reveals that the signal of ENSO can better indicate the precipitation of Guangdong during the DBRP in 1977−2001 but its indication decreases during recent years. It also reveals that the SSTA of tropical southeast Atlantic in spring may have been the key factor which influences the anomaly of precipitation in Guangdong during the DBRP in recent years. During the years with warm SEA, precipitation during the DBRP possibly exceeds the climate state. The SSTA of tropical southeast Atlantic may influence the precipitation in Guangdong through the Gill response in the tropics and the wave train at mid - and high-latitudes. However, the mechanism remains to be further studied.

REFERENCES

[1] WU S S, LIANG J Y. Temporal and spatial characteristics of the drought and flood during the rainy season in South China [J]. Journal of Tropical Meteorology (in Chinese), 1992, 8(1): 87-92.

[2] ZHAO Z H, CHEN C M. Features and types of spatial-temporal distribution of the rainfall from May to September in Guangdong [J]. Acta Scientiarum Naturalium Universitatis Sunyatseni（in Chinese),1997, 36(2): 92-96.

[3] ZHENG B, LIANG J Y, LIN A L, et al. Frontal rain and summer monsoon rain during pre-rainy season in South China, Part I: Determination of the division dates [J]. Chinese Journal of Atmospheric Sciences (in Chinese), 2006, 30(6): 1207-1216, https://doi. org / 10.3878 / j. issn.1006-9895.2006.06.15

[4] XIN F, XIAO Z N, LI Z C. Relation between flood season precipitation anomalies in South China and East Asian atmospheric low frequency oscillation in 1997 [J]. Meteorological Monthly (in Chinese), 2007, 33(12): 23-30, https://doi.org/10.7519/j.issn.1000-0526.2007.12.004

[5] GU D J, JI Z P. The strong dragon-boat precipitation of Guangdong in 2008 and quasi-10-day oscillation [J]. Journal of Tropical Meteorology (in Chinese), 2011, 27(1): 11-21, https://doi. org / 10.3969 / j. issn. 1004-4965.2011.01.002

[6] LI L P, ZHOU L, YU Z X. Interdecadal anomaly of rainfall during the first rainy season in South China and its possible causes [J]. Transactions of Atmospheric Sciences (in Chinese), 2018, 41(2): 186-197, https://doi.org/10.13878/j.cnki.dqkxxb.20160224001

[7] QIAN G M, LV Y P, DU Y D, et al. Technical manual for climate operation of Guangdong Province [M]. Beijing: China Meteorological Press, 2008: 37-50 (in Chinese).

[8] ZHANG T, WEI F Y, HAN X. Low frequency oscillations of southern hemispheric critical systems and precipitation during flood season in South China [J]. Journal of Applied Meteorological Science (in Chinese), 2011, 22(3): 265-274.

[9] CHEN Y, ZHAI P M. Persistent extreme precipitation events in China during 1951-2010 [J]. Climate Research, 2013, 57(2): 143-155, https://doi.org/10.3354/cr01171

[10] TANG Y B, GAN J J, ZHAO L, et al. On the climatology of persistent heavy rainfall events in China [J]. Advances in Atmospheric Sciences, 2006, 23(5): 678-692, https://doi.org/10.1007/s00376-006-0678-x

[11] HUANG Z Z, WANG H, CHEN X G, et al. Characteristics of "Dragon Boat Water" and its impact on the early rice yield under climate change [J]. Ecology and Environmental Sciences (in Chinese), 2011, 20(5): 793-797, https://doi. org / 10.16258 / j. cnki. 1674-5906.2011.05.010

[12] LI C H, JIANG G H, WANG T, et al. The analysis of the strongest dragon-boat rain in Guangdong province in 2008 [J]. Journal of Anhui Agricultural Sciences (in Chinese), 2009, 37(28): 3739-3741, https://doi. org / 10.13989/j.cnki.0517-6611.2009.28.053

[13] LIN L X, WU N G, HUANG Z, et al. Causality analysis of the infrequent dragon-boat precipitation in Guangdong province in 2008 [J]. Meteorological Monthly (in Chinese), 2009, 35(4): 43-50, https://doi. org / 10.7519 / j. issn.1000-0526.2009.4.006

[14] WU H Y, LI C M, WANG D L. Analysis on characteristics and abnormal causes of dragon-boat precipitation in Guangdong in the past 55 years [J]. Journal of Tropical Meteorology (in Chinese), 2017, 33(5): 608-616, https://doi.org/10.16032/j.issn.1004-4965.2017.05.004

[15] GU D J, ZHANG W. The strong dragon boat race precipitation of Guangdong in 2008 and quasi-10-day oscillation [J]. Journal of Tropical Meteorology, 2012, 18 (3): 349-359, https://doi. org / 10.16555 / j. 1006-8775.2012.03.009

[16] WEN Z P, DONG L Y, WU L J, et al. The characteristics of 30-60 day oscillation and its relation to the durative rainstorm in Guangdong [J]. Acta Scientiarum Naturalium Universitatis Sunyatseni (in Chinese), 2007, 46(5): 98-103.

[17] HU Y M, DU Y D, LUO X L. Precipitation patterns during the "dragon boat water" in South China for the recent 49 years [J]. Meteorological Monthly (in Chinese), 2013, 39(8): 1031-1041, https://doi. org / 10.7519 / j. issn.1000-0526.2013.08.010

[18] CHEN S, GAO J Y, HUANG L N, et al. Decadal variation characteristics of South China pre-flood season persistent rainstorm and its mechanism [J]. Journal of Applied Meteorological Science (in Chinese), 2017, 28(1): 86-97, https://doi.org/10.11898/1001-7313.20170108

[19] LIN A L, LI C H, GU D J, et al. Impact of tropical intraseasonal oscillations on the precipitation of Guangdong in Junes [J]. Journal of Tropical Meteorology (in Chinese), 2013, 29(3): 353-363, https://doi. org / 10.3969/j.issn.1004-4965.2013.03.001

[20] MA H, CHEN Z H, JIANG L P, et al. SVD analysis between the annually first raining period precipitation in the south of China and the SST over offshore waters in China [J]. Journal of Tropical Meteorology (in Chinese), 2009, 25(2): 241-245.

[21] YANG J L, LIU Q Y, XIE S P, et al. Impact of the Indian Ocean SST basin mode on the Asian summer monsoon [J]. Geophysical Research Letters, 2007, 34: L02708, https://doi.org/10.1029/2006GL028571

[22] LI S L, LU J, HUANG G, et al. Tropical Indian Ocean basin warming and East Asian summer monsoon: A multiple AGCM study [J]. Journal of Climate, 2008, 21 (22): 6080-6088, https://doi.org/10.1175/2008JCLI2433.1

[23] CHAN J C L, ZHOU W. PDO, ENSO and the early summer monsoon rainfall over south China [J]. Geophysical Research Letters, 2005, 32: L08810, https://doi.org/10.1029/2004GL022015

[24] HONG W, REN X J. Persistent heavy rainfall over South China during May-August: Subseasonal anomalies of circulation and sea surface temperature [J]. Acta Meteorologica Sinica, 2013, 27(6): 769-787, https://doi.org/10.1007/s13351-013-0607-8

[25] ZHOU W, LI C, CHAN J C L. The interdecadal variations of the summer monsoon rainfall over South China [J]. Meteorology and Atmospheric Physics , 2006, 93(4): 165-175, https://doi.org/10.1007/s00703-006-0184-9

[26] CHANG C P, ZHANG Y S, LI T. Interannual and interdecadal variations of the East Asian summer monsoon and tropical Pacific SSTs. Part II: Meridional structure of the monsoon [J]. Journal of Climate, 2000, 13 (24): 4326-4340, https://doi.org/10.1175/1520-0442(2000)013<4326:IAIVOT>2.0.CO;2

[27] YIM S Y, YEH S W, WU R G, et al. The influence of ENSO on decadal variations in the relationship between the East Asian and western North Pacific summer monsoons [J]. Journal of Climate, 2008, 21(13): 3165-3179, https://doi.org/10.1175/2007JCLI1948.1

[28] KALNAY E, KANAMITSU M, KISTLER R, et al. The NCEP/NCAR 40-year reanalysis project [J]. Bulletin of the American Meteorological Society, 1996, 77(3): 437-472, https://doi.org/10.1175/1520-0477(1996)077<0437:TNYRP>2.0.CO;2

[29] RAYNER N A, PARKER D E, HORTON E B, et al. Global analyses of sea surface temperature, sea ice, and night marine air temperature since the late nineteenth century [J]. Journal of Geophysical Research, 2003, 108 (D14): 4407, https://doi.org/10.1029/2002JD002670

[30] TAKAYA K, NAKAMURA H. A formulation of a phase-independent wave-activity flux for stationary and migratory quasigeostrophic eddies on a zonally varying basic flow [J]. Journal of the Atmospheric Sciences, 2001, 58(6): 608-627, https://doi.org/10.1175/1520-0469(2001)058<0608:AFOAPI>2.0.CO;2

[31] ZHANG D Q, CHEN L J, LIU Y J, et al. Review on the failure of precipitation prediction in October 2016 [J]. Meteorological Monthly (in Chinese), 2018, 44(1): 189-198, https://doi.org/10.7519/j.issn.1000-0526.2018.01.017

[32] LIN A L, LIANG J Y, LI C H, et al. Monsoon circulation background of '0506' continuous rainstorm in South China [J]. Advances in Water Science (in Chinese), 2007, 18(3): 424-432.

[33] HUANG R H, SUN F Y. Impacts of the thermal state and the convective activities in the tropical western warm pool on the summer climate anomalies in East Asia [J]. Chinese Journal of Atmospheric Sciences (in Chinese), 1994, 18(2): 141-151, https://doi.org/10.3878/j.issn.1006-9895.1994.02.02

[34] WANG H M, LIU G, PENG J B, et al. Preliminary study on the effect of intraseasonal evolution of the tropical Atlantic SST anomalies on summer persistent heatwave events over the area south of the Yangtze River [J]. Chinese Journal of Atmospheric Sciences (in Chinese), 2021, 45(2): 300-314, http://dx.doi.org/10.3878/j.issn.1006-9895.2005.19235

[35] QIANG X M, YANG X Q. Relationship between the first rainy season precipitation anomaly in South China and the sea surface temperature anomaly in the Pacific [J]. Chinese Journal of Geophysics (in Chinese), 2013, 56(8): 2583-2593, https://doi.org/10.6038/cjg20130808

[36] MIAO R, WEN M, ZHANG R H. Persistent precipitation anomalies and quasi-biweekly oscillation during the annually first rainy season over South China in 2010 [J]. Journal of Tropical Meteorology (in Chinese), 2017, 33 (2): 155-166, https://doi.org/10.16032/j.issn.1004-4965.2017.02.002

[37] WANG B, WU R G, FU X H. Pacific-East Asian teleconnection: How does ENSO affect East Asian climate? [J]. Journal of Climate, 2000, 13(9): 1517-1536, https://doi.org/10.1175/1520-0442(2000)013<1517:PEATHD>2.0.CO;2

[38] XIE S P, HU K M, HAFNER J, et al. Indian Ocean capacitor effect on Indo-Western Pacific climate during the summer following El Niño [J]. Journal of Climate, 2009, 22(3): 730-747, https://doi.org/10.1175/2008JCLI2544.1

[39] WALLACE J M, GUTZLER D S. Teleconnections in the geopotential height field during the Northern Hemisphere winter [J]. Monthly Weather Review, 1981, 109(4): 784-812, https://doi.org/10.1175/1520-0493(1981)109<0784:TITGHF>2.0.CO;2

[40] LIU H B, WEN M, HE J H, et al. Characteristics of the northeast cold vortex at intraseasonal time sacal and its impact [J]. Chinese Journal of Atmospheric Sciences (in Chinese), 2012, 36(5): 959-973, https://doi.org/10.3878/j.issn.1006-9895.2012.11167

[41] GILL A E. Some simple solutions for heat-induced tropical circulation [J]. Quarterly Journal of the Royal Meteorological Society, 1980, 106(449): 447-462, https://doi.org/10.1002/qj.49710644905

Citation: DONG Shao-rou, YANG Song, LIU Wei, et al. Analysis of Precipitation Anomaly and a Failed Prediction During the Dragon-boat Rain Period in 2022 [J]. Journal of Tropical Meteorology, 2023, 29(1): 115-127, https://doi.org/10.46267/j.1006-8775.2023.009